Z. Phys. Chem. **227** (2013) 1281–1299 / **DOI** 10.1524/zpch.2013.0407

Simultaneous Measurement of Reactive and Inelastic Scattering: Differential Cross Section of the $H + HD \rightarrow HD(v', j') + H$ Reaction

By Justin Jankunas[1], Mahima Sneha[1], Richard N. Zare[1,*], Foudhil Bouakline[2], and Stuart C. Althorpe[3]

[1] Department of Chemistry, Stanford University, Stanford, California 94305-5080, USA
[2] Max Born Institute, Max Born Strasse 2a, 12489 Berlin, Germany
[3] Department of Chemistry, University of Cambridge, Lensfield Road, Cambridge CB2 1EW, UK

(Received February 28, 2013; accepted May 4, 2013)
(Published online August 5, 2013)

Reaction Dynamics / $H + H_2$ / Differential Cross Section / Geometric Phase

The $H + HD \rightarrow HD(v', j') + H$ reaction has been studied experimentally and theoretically. Differential cross sections of $HD(v', j')$ products have been measured by means of a Photoloc technique and calculated using a time-independent quantum mechanical theory. Three product states: $HD(v' = 1, j' = 8)$ at a collision energy (E_{coll}) of 1.97 eV; $HD(v' = 2, j' = 3)$ at $E_{coll} = 1.46$ eV; and $HD(v' = 2, j' = 5)$ at $E_{coll} = 1.44$ eV, show very good agreement between theory and experiment. The other two, highly rotationally excited states studied, $HD(v' = 1, j' = 12)$ and $HD(v' = 1, j' = 13)$ at $E_{coll} = 1.97$ eV, exhibit a noticeable disagreement between experiment and theory. This is consistent with our most recent findings on the $H + D_2 \rightarrow HD(v', j') + D$ reaction, wherein the differential cross sections of $HD(v' = 1$, high $j')$ product states showed similar disagreement between the experiment and theory [J. Jankunas, M. Sneha, R. N. Zare, F. Bouakline, and S. C. Althorpe, J. Chem. Phys. **138** (2013) 094310]. In all five cases, however, we find overwhelming support that the experimental signal is a sum of reactive and inelastic scattering events. The interference term escapes detection, frustrating our attempt to observe geometric phase effects. Nevertheless, this work constitutes a first experimental example in which the indistinguishability of reactive and inelastic channels must be taken into account explicitly when constructing differential cross sections.

1. Introduction

The hydrogen exchange reaction, most generally abbreviated as $H + H_2$, has appeared on the scene of reaction dynamics under several different guises. The two most common ones are $H + D_2$ and $D + H_2$ because this choice of isotopologues allows the distinction between reactants and products in both reactive and inelastic scattering to be easily made. In case of a reactive collision both $H + D_2$ and $D + H_2$ reactions

* Corresponding author. E-mail: zare@stanford.edu

yield HD as a product, which nearly removes the experimental background. Indeed, this is part of the reason why the reactive scattering of the $H + D_2$ and $D + H_2$ reactions has received considerably more experimental attention than the inelastic process. It is well known that reactive encounters between a hydrogen atom and a hydrogen molecule are mostly direct in nature [1–8]. According to this model, small-impact-parameter collisions lead to rotationally cold, backward scattered products, while glancing, large-impact-parameter collisions produce rotationally excited, sideways/forward scattered products. A different reaction mechanism has been discovered for highly internally excited $HD(v', j')$ products of the $H + D_2 \rightarrow HD(v', j') + D$ reaction, wherein rotationally excited molecules become more backward scattered than the rotationally cold ones [9,10]. In addition, highly internally excited $HD(v', j')$ products, particularly the $HD(v' = 4,\ j')$ manifold, exhibit a more isotropic angular distribution [9–12]. The deuterium atom Rydberg tagging technique was employed in the study of an $H + HD \rightarrow H_2(v', j') + D$ hydrogen exchange variant [13,14], where the forward peak has been attributed to the well-known time-delayed mechanism observed in the $H + D_2 \rightarrow HD(v' = 2, 3,\ j' = 0) + D$ reaction [8,15–19]. Finally, Kliner *et al.* [20] have studied the $H + \textit{para}\text{-}H_2 \rightarrow \textit{ortho}\text{-}H_2(v', j') + H$ reaction. The selection rule forbidding *ortho-para* intraconversion excludes any contribution from the inelastic processes and hence the experimental signal is purely reactive. In other words, the incoming hydrogen atom projectile necessarily replaces one of the hydrogen atoms initially bound in the diatomic molecule.

The dynamics of inelastic $H + H_2$ scattering, on the other hand, is very different from its reactive counterpart. Rotational state distributions, for example, are relatively insensitive to the collision energy or vibrational quantum number of the product [21]. Furthermore, inelastic $H + D_2 \rightarrow D_2(v', j') + H$ encounters take place at relatively larger impact parameters, as compared to analogous $H + D_2 \rightarrow HD(v', j') + D$ reactive collisions. According to this picture, the $D_2(v', j')$ product is internally excited *via* a bond stretch rather than a bond compression, wherein a hydrogen atom "fails" to capture one of the D atoms and the D_2 molecule snaps back into a vibrationally excited state in a frustrated, aborted chemical reaction. This is the underpinning of a so-called tug-of-war mechanism [22–25].

We were therefore eager to introduce yet another character into the $H + H_2$ saga by studying the $H + HD \rightarrow HD(v', j') + H$ reaction. Unlike all previous studies of hydrogen exchange reaction that examined either reactive or inelastic scattering, $H + HD \rightarrow HD(v', j') + H$ reaction achieves both! If one could label hydrogen atoms, one could distinguish between the reactive and inelastic processes, *i.e.*,

$$H_a + H_bD \rightarrow H_aD(v', j') + H_b \tag{1a}$$

$$H_a + H_bD \rightarrow H_bD(v', j') + H_a \tag{1b}$$

where Eq. (1a) denotes a reactive scattering (the two hydrogen atoms "switch" places) and Eq. (1b) represents an inelastic scattering. Although theoretically one can study the two processes independently and derive the corresponding reactive and inelastic scattering amplitudes, f_R and f_{NR}, respectively, experimentally $H_aD(v', j')$ and $H_bD(v', j')$ molecules are indistinguishable. Particle indistinguishability is a well-known quantum mechanical effect. The differential cross section (DCS) for an elastic scattering of two

identical particles wherein only one of the particles is detected at some angle θ is given by [26]

$$\frac{d\sigma}{d\Omega} = |f(\theta) \pm f(\pi - \theta)|^2 \tag{2}$$

where $f(\theta)$ is the scattering amplitude into an angle θ, and the upper and lower signs refer to even and odd total spin of colliding particles, respectively. In the case of the H + HD reaction it is more convenient to talk in terms of f_R and f_{NR} amplitudes. Miller and co-workers [27] have shown that a reaction of the A + AB → AB + A type has a cross section given by

$$\frac{d\sigma}{d\Omega} = \frac{1}{2}(1+\lambda)|f_R + f_{NR}|^2 + \frac{1}{2}(1-\lambda)|f_R - f_{NR}|^2 \tag{3}$$

where $\lambda = (-1)^{2s}/(2s+1)$ and s is the nuclear spin of the A-atom. A hydrogen atom has a nuclear spin of one-half and Eq. (3) reduces to

$$\frac{d\sigma}{d\Omega} = |f_R|^2 + |f_{NR}|^2 + \frac{1}{2}\left(f_{NR}^* f_R + f_R^* f_{NR}\right) \tag{4}$$

Equation (4) has a straightforward interpretation. State-specific detection of HD(v', j') as a product of the H + HD → HD(v', j') + H reaction will contain an incoherent sum of reactive and inelastic scattering contributions, $|f_R|^2 + |f_{NR}|^2$, respectively, and a cross term, the last entry in Eq. (4). The H + HD → HD(v', j') + H reaction is therefore interesting in several respects. First, and to the best of our knowledge, there have been no experimental measurements of chemical reactions wherein both $|f_R|^2$ and $|f_{NR}|^2$ were measured simultaneously. Second, the cross term in Eq. (4) is even more informative. As has been first shown by Mead [28], the signature of a geometric phase (GP) effect in the case of $H + H_2 \rightarrow H_2 + H$, or H + HD → HD + H, is to change the sign of the interference term in Eq. (4). Unfortunately, the cross term is of a highly oscillatory nature and has turned out to be beyond our experimental resolution for the states studied.

The details of the experimental procedure are discussed in Sect. 2; Sect. 3 presents the theoretical method used; Sect. 4 contains the experimental results; Sect. 5 is an ensuing discussion; and Sect. 6 presents conclusions.

2. Experimental

A detailed description of an experimental set-up has been given elsewhere [8,9,29] and only the most pertinent details are described herein. Table 1 summarizes the main experimental parameters of this work. A 5% HBr (99.9%, Praxair) in HD (D, 97%, Cambridge Isotope Laboratories Inc.) mixture was expanded supersonically through a 0.76 mm diameter nozzle (General Valve, Series 9) at a backing pressure of ∼ 1300 Torr. The skimmed (2 mm skimmer, Beam Dynamics) molecular beam was intersected perpendicularly with either one or two, *vide infra*, gently focused laser beams. The HBr photolysis as well as HD ionization took place in the extraction region of a Wiley–McLaren time-of-flight (TOF) mass spectrometer. The HD^+ ions were collected on a position-sensitive delay line detector.

Table 1. Main experimental parameters for different HD(v', j') product states studied. The first number in column 3 is the probe laser power and the second one is the photolysis laser power. The HD($v' = 1, j'$) states do not have offline REMPI values in column 6 because these product states were studied under two-laser conditions; see experimental section for more details.

HD(v', j') state	E_{coll}, eV	Laser power, power, μJ	Number of ions	REMPI (online) ±6 pm, nm	REMPI (offline) ±6 pm, nm	Photoloc speed range, m/s	Observed peak, m/s	HD recoil speed, m/s
(1, 8)	1.86	400/400	6693	211.855	N/A	1344 – 9557	4450	192
(1, 12)	1.86	400/450	8195	214.988	N/A	2174 – 8727	6150	196
(1, 13)	1.86	500/450	4019	215.918	N/A	2453 – 8448	6100	197
(2, 3)	1.46	500	11 412	217.333	217.261	1914 – 7738	3100	182
(2, 5)	1.44	550	9176	218.000	217.921	2186 – 7424	4300	183

The required ultraviolet (UV) laser light was obtained by either frequency tripling the output of a dye laser (Lambda Physik, LPD 3000) pumped by the second harmonic of an Nd:YAG^{3+} laser (Spectra Physics, GCR Series), or by frequency doubling the output of a dye laser (Lambda Physik, LPD 3000) pumped by the third harmonic of an Nd:YAG^{3+} laser (Quanta-Ray, DCR-3). All frequency mixing was carried out in BBO crystals.

The HD(ν', j') product was ionized state-selectively by means of a [2+1] resonance enhanced multiphoton ionization (REMPI) technique *via* the Q(j') branch members of the $(0, \nu')$ vibrational band of the $E, F^1\Sigma_g^+ - X^1\Sigma_g^+$ electronic transition. The HD($\nu' = 1, j' = 8$), HD($\nu' = 1, j' = 12$) and HD($\nu' = 1, j' = 13$) product states were studied under two-laser conditions. A dedicated photolysis laser, focused with a 50 cm lens, was used to photodissociate the hydrogen bromide molecule to yield fast H atoms. The probe laser, focused with a 60 cm lens, probed the HD(ν', j') reaction products. Because the probe laser can also photodissociate the HBr and ionize the HD(ν', j') products, a background subtraction was carried out. This was done by firing the photolysis laser $\sim$15 ns before the probe and $\sim$50 ns after the probe laser. The former situation gives rise to all the background signal plus the desired HD(ν', j') signal, we call it 'Signal 2'. When the photolysis laser is fired after the probe laser, then only the background signal is observed. We call this signal 'Signal 1'. The true experimental signal is therefore obtained by subtracting 'Signal 1' from 'Signal 2', *i.e.*, 'True signal' = 'Signal 2' − 'Signal 1'. In this case the photolysis laser wavelength was set to $\lambda_{\text{photolysis}} = 198.5$ nm, corresponding to a center-of-mass H + HD collision energy of 1.86 eV.

The HD($\nu' = 2,\ j' = 3$) and HD($\nu' = 2,\ j' = 5$) products were studied under one-laser conditions. In this case, a laser was parked on a desired REMPI line and its wavelength was scanned over the Doppler profile of a molecule, ± 6 pm. We call this an 'online scan'. Next, the laser wavelength was moved off the REMPI line and it was again scanned for ± 6 pm. We call this an 'offline scan' as it corresponds to the background scan. Similar to two-laser conditions, 'True signal' = 'online scan' − 'offline scan'. The collision energy in this case was determined by the REMPI wavelength. In the case of HD($\nu' = 2,\ j' = 3$) $E_{\text{coll}} = 1.46$ eV while for HD($\nu' = 2,\ j' = 5$) $E_{\text{coll}} = 1.44$ eV. All wavelengths were measured with a laser wavelength meter (Wavemaster, Coherent).

3. Theory

We obtained the exchange-symmetrised DCS of Eq. (4) by computing the (non-exchange-symmetrised) scattering amplitudes f_{NR} and f_R using the ABC code of Skouteris *et al.* [30], with the refined Boothroyd–Keogh–Martin–Peterson (BKMP2) potential energy surface [31]. Separate calculations were performed for each initial rotational quantum number $j = 0$, 1, and 2 of the reactant HD molecule, and for each total parity of the triatomic molecule, and repeated for each partial wave up to a total angular momentum $J = 55$. To solve the coupled-channel hyperradial equations, the maximum value of the hyperradius $\rho_{\max}$ was set to 25 a_0, and 250 sectors were used; the coupled-channel basis-set parameters were set to $E_{\max} = 2.85$ eV, $j_{\max} = 20$ and $k_{\max} = 10$. These parameters were sufficient to achieve convergence of the DCS across the range of collision energies considered here. The convergence was double-checked by comparing the $j = 0$ DCS with the results of wavepacket [32] calculations (not shown here); the two sets of results were in very close agreement.

Consideration of the geometric phase effect is rather subtle. From previous work [30–38], we know that the non-exchange-symmetrised nuclear wavefunction does not encircle the CI at the collision energies considered here, which are far below the

energetic minimum of the conical intersection (CI) at 2.74 eV. Hence geometric phase (GP) effects did not need to be taken into account in the calculations of f_{NR} and f_R. However, the act of symmetrising the wave function (with respect to exchange of the H-atoms) causes it to encircle the CI (as can be easily demonstrated by sketching the form of the symmetrised wave function in hyperspherical coordinates). As a result, GP effects need to be included when superposing f_{NR} and f_R in Eq. (4). Mead [28] showed that the sole effect of the GP in such a case is to change the sign of f_{NR} relative to f_R; see Sect. 5.

4. Results

In a Photoloc experiment the angular information is obtained by measuring the laboratory speed distribution, which is then converted into a DCS *via* the law of cosines [39]. The key experimental step is therefore an accurate measurement of HD product molecular speeds. Figure 1 shows a typical laboratory speed distribution of HD($v' = 2$, $j' = 3$) product at $E_{\text{coll}} = 1.46$ eV. There are two traces in Fig. 1a – the 'online' and the 'offline' one. The 'offline' scan is the background, wherein the laser wavelength was not resonant with any HD(v', j') $[2+1]$ REMPI line. As is evidenced by Fig. 1a, the background subtraction procedure is well warranted as there is a substantial signal in the Photoloc speed range even when in the nonresonant ionization regime. We have not established the source of the nonresonant ionization background, but we suspect it might be from the nonresonant ionization of HD products in all internal states in which they are formed. The 'online' scan corresponds to a resonant ionization of the reaction product HD($v' = 2$, $j' = 3$). Ideally, one would expect the 'offline' and 'online' signals to be the same everywhere except the Photoloc range in which the only 'extra' signal arises from the HD($v' = 2$, $j' = 3$) reaction product. It is quite striking that this ideal situation is borne out experimentally, *i.e.*, the 'online' and 'offline' traces are almost identical at all speeds but in the Photoloc range (Fig. 1a). This makes us very confident in our experimental method, that is, we are removing all background ionization contributions to the observed signals. We would also like to point out the peak at around ~ 1300 m/s in Fig. 1a. It corresponds to a nonresonant ionization of the HD($v' = 0$, low j') species that comprise about 95% of the molecular beam.

Figure 1b shows the difference between the 'online' and 'offline' scans. In other words, this is the true speed distribution of the HD($v' = 2$, $j' = 3$) reaction product. This speed distribution is converted into an angular HD($v' = 2$, $j' = 3$) distribution *via* the familiar law of cosines. The resultant DCSs (for a range of different v' and j') are pictured in Figs. 2–6. Each HD(v', j') product state has three associated DCSs: one containing the fit of experimental data to an incoherent sum of reactive and inelastic scattering, abbreviated as $|f_R|^2 + |f_{NR}|^2$; one containing a fit to only the reactive scattering, $|f_R|^2$; and one containing a fit to only the inelastic scattering, $|f_{NR}|^2$. The experimental data is a mean of three to six scans, and the associated y-axis error bars correspond to one standard deviation. In each figure the experimental DCS represents a relative differential cross section which is scaled to each theoretical curve in a manner discussed below.

Theoretical calculations have been blurred to simulate the experimental conditions better. Each curve in Figs. 2–6 has been smoothed with a Gaussian to account

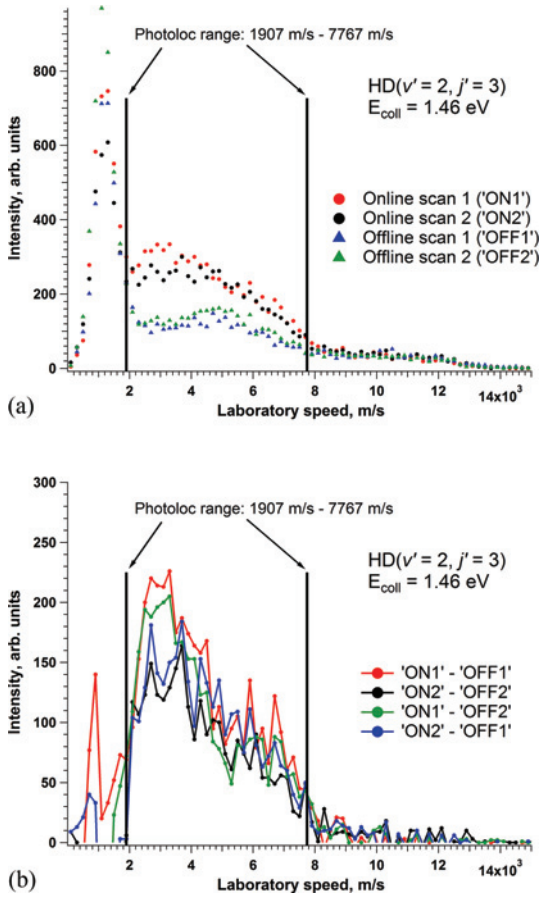

Fig. 1. Laboratory speed distributions of HD($v' = 2, j' = 3$) product at $E_{\text{coll}} = 1.46$ eV. **(a)** Red and black circles represent an 'online' scan, *i.e.* laser wavelength parked on HD($v' = 2, j' = 3$) REMPI line, and blue and green triangles are 'offline' speed distributions, *i.e.* laser wavelength off resonance with any (known) HD(v', j') REMPI line. Vertical lines indicate the photoloc-allowed range of HD($v' = 2, j' = 3$) speeds. **(b)** Corrected experimental signal obtained by subtracting the 'offline' speed distribution from the 'online' one. The dot-connecting lines are an eye aid only. Both **(a)** and **(b)** panels have the same ordinate scale.

for a 0.05 eV spread in the collision energy. The theoretical curves have been properly weighted to account for the spread in the initial rotational states of HD reactant. Rotational blurring proved to be minor in the case of reactive $\text{H} + \text{HD}(v = 0, j) \rightarrow \text{HD}(v', j') + \text{H}$ scattering. Quite surprisingly, however, the initial rotational state of HD reactant turned out to have a huge effect on the overall shape of the DCSs for inelastic $\text{H} + \text{HD}(v = 0, j) \rightarrow \text{HD}(v', j') + \text{H}$ collisions. These effects are illustrated in Fig. 7. To weigh the theoretical calculations correctly, we have measured the rotational state distribution of HD reactant, and found that $\sim 33\%$ of the population resides in HD($v = 0, j = 0$), $\sim 37\%$ in HD($v = 0, j = 1$) and $\sim 20\%$ in HD($v = 0, j = 2$). This corresponds to a rotational temperature of 190 K. The remaining 10% of

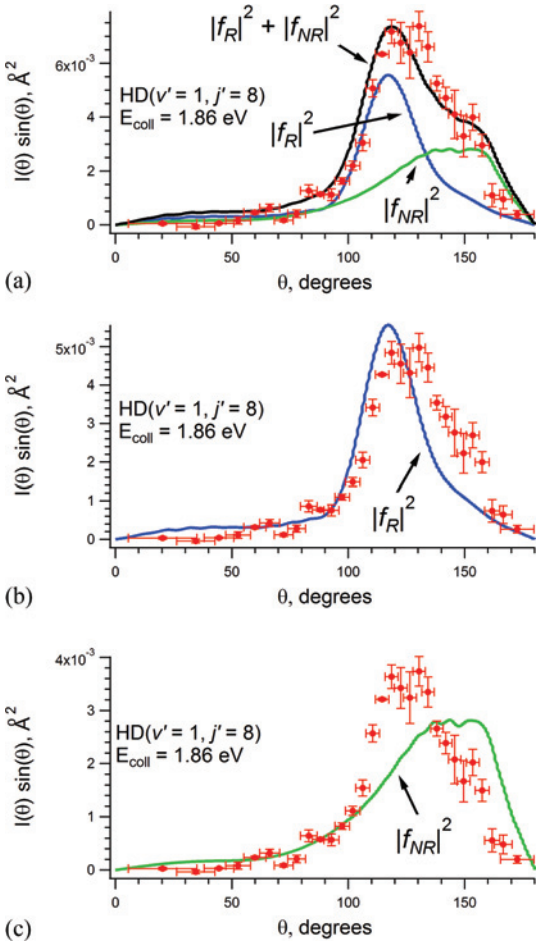

Fig. 2. DCS for $H + HD \rightarrow HD(v' = 1, j' = 8) + H$ reaction product. Each state has three fits: reactive + inelastic, $|f_R|^2 + |f_{NR}|^2$ (black curve), reactive, $|f_R|^2$ (blue curve), and inelastic, $|f_{NR}|^2$ (green curve). Red dots are experimental measurements that correspond to an average measurement of three to six independent scans, and the y-axis error bars are an associated standard deviation of three to six experimental trials. The x-axis error bars reflect the inherent uncertainty in the $HD(v', j')$ laboratory speed due to the ionization recoil of HD^+. Solid curves are blurred TI-QM calculations. A superior $|f_R|^2 + |f_{NR}|^2$ fit is evident in all cases.

HD reactant molecules were found in $HD(v = 0, j \geq 3)$ states. We have excluded these more rotationally excited reactants from further consideration. We also believe that 10% is a small enough number to be not very significant. Indeed, similar conclusions were reached by Fernandez-Alonso *et al.* [40] who measured the $D_2(v = 0, j)$ reactant rotational state distribution and found that about 10% of the population resides in $D_2(v = 0,\ j > 2)$ states. Subsequently, all theoretical calculations on $H + D_2$ reaction were performed assuming only three initial reactant states, *i.e.*, $D_2(v = 0, j \leq 2)$, and the agreement in most cases was found to be very good [7–9].

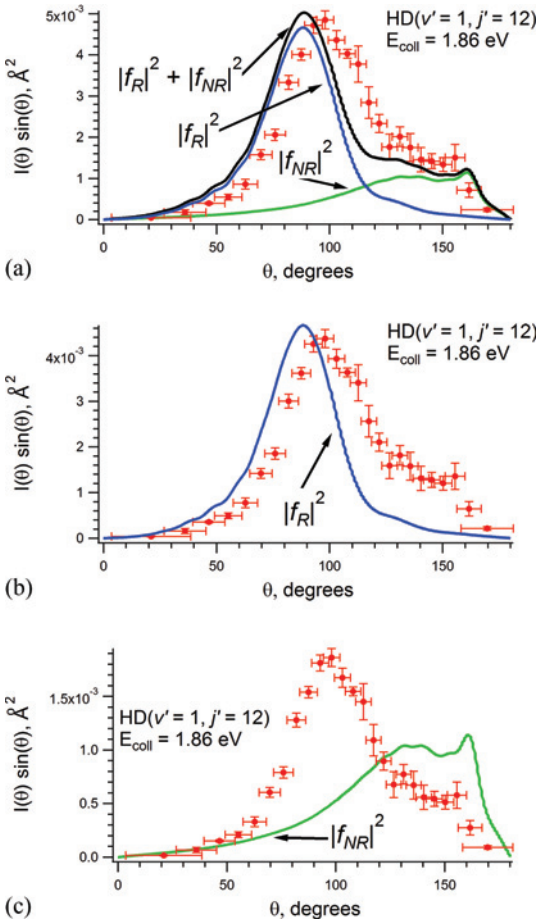

Fig. 3. Same as Fig. 2 but for HD($\nu' = 1, j' = 12$) + H reaction product.

The last source of uncertainty in the experimental measurement of HD(ν', j') laboratory speed is the HD^+ recoil imparted by the departing electron. This uncertainty is a fundamental limitation to our experimental speed resolution that cannot be eliminated using a [2 + 1] REMPI scheme *via* the E, F state. Actual recoil values are tabulated in Table 1. In our earlier studies this inherent uncertainty in the speed of HD(ν', j') product was taken into account by convoluting the theoretical calculations with a ~ 200 m/s wide Gaussian, *i.e.*, typical HD^+ recoil values, see Table 1 [7–9]. Here we add the appropriate error bars on experimentally measured points rather than further blurring theoretical calculations. In a Photoloc experiment the center-of-mass scattering angle θ is given by [39]

$$\theta = \cos^{-1}\left[\frac{u_{\mathrm{COM}}^2 + u_{\mathrm{HD}}^2 - v_{\mathrm{LAB}}^2}{2u_{\mathrm{COM}}u_{\mathrm{HD}}}\right] \tag{5}$$

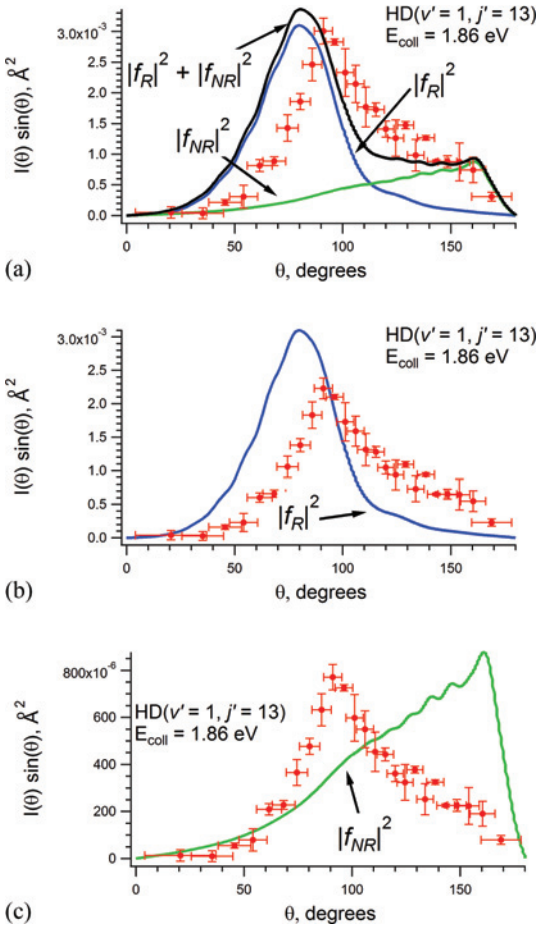

Fig. 4. Same as Fig. 2 but for HD($v' = 1, j' = 13$) + H reaction product.

Where u_{COM}, u_{HD}, and v_{LAB} are the center-of-mass velocity, HD(v', j') velocity in the center of mass and HD(v', j') velocity in the laboratory frame, respectively. The uncertainty associated with the center-of-mass velocity, corresponding to an uncertainty of 0.05 eV in E_{coll}, has been already taken into account by blurring theoretical calculations with an appropriate Gaussian, *vida supra*. Hence only v_{LAB} has an explicit, *i.e.*, $\pm v_{\mathrm{recoil}}$, error appearing in Eq. (5). To translate the error from v_{LAB} into θ, *i.e.*,

$$\Delta\theta = \left(\frac{\partial\theta}{\partial v_{\mathrm{LAB}}}\right)\Delta v_{\mathrm{LAB}} \tag{6}$$

we differentiate Eq. (5) with respect to v_{LAB}, *i.e.*,

$$\Delta\theta = \frac{2v_{\mathrm{LAB}}}{\sqrt{4u_{\mathrm{COM}}^2 u_{\mathrm{HD}}^2 - (u_{\mathrm{COM}}^2 + u_{\mathrm{HD}}^2 - v_{\mathrm{LAB}}^2)^2}}\Delta v_{\mathrm{LAB}} \tag{7}$$

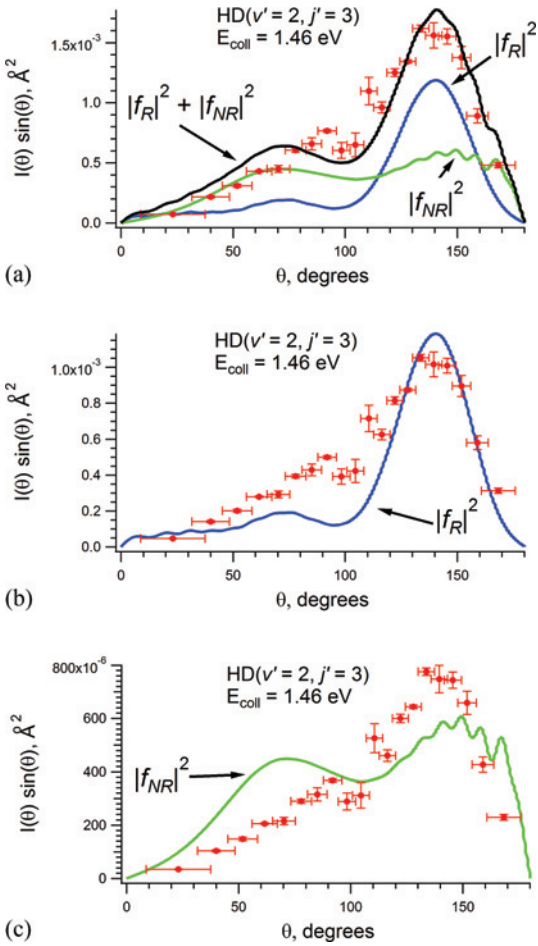

Fig. 5. Same as Fig. 2 but for HD($\nu' = 2$, $j' = 3$) + H reaction product.

A few things should be noted about the $\Delta\theta$ behavior. Firstly, $\Delta\theta$ depends on ν_{LAB}, *i.e.*, backward, sideway, and forward directions will have different uncertainties in θ. Secondly, $\Delta\theta$ is singular when

$$|\mathbf{v}_{\mathrm{LAB}}| = |\mathbf{u}_{\mathrm{COM}}| \pm |\mathbf{u}_{\mathrm{HD}}| \tag{8}$$

In other words, $\Delta\theta$ will be large for very backward and very forward directions. Consequently, $\Delta\theta$ will be the smallest for $\theta \sim 90°$. This behavior is clearly seen in Figs. 2–6.

Finally, we apply the least-squares analysis to quantify the fits in Figs. 2–6. We have introduced this method in our recent work on $\mathrm{H} + \mathrm{D}_2 \rightarrow \mathrm{HD}(\nu', j') + \mathrm{H}$ reaction [41]. Briefly, because the experiment measures relative cross sections while theoretical calculations yield absolute values, one is free to multiply the experimental values by an arbitrary constant F to bring theory and experiment into as close of an agreement as

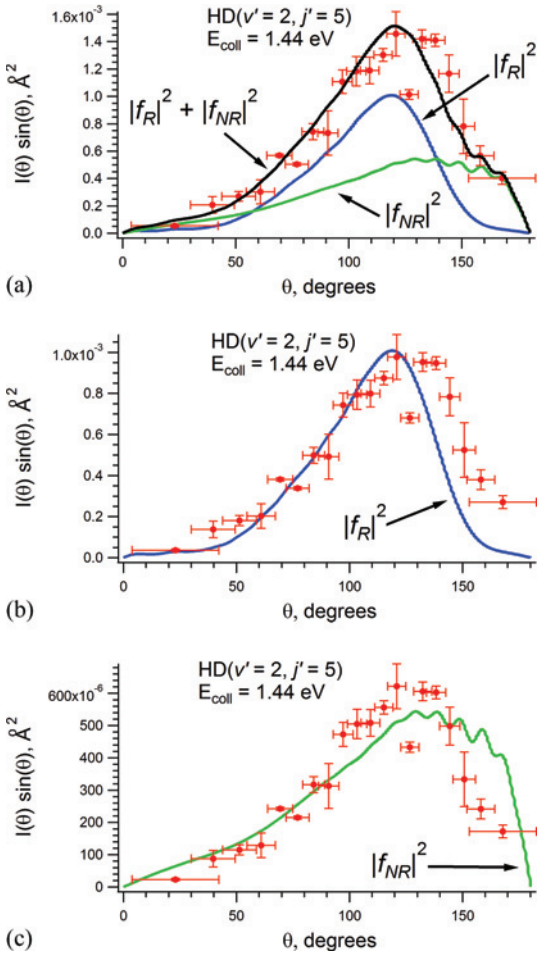

Fig. 6. Same as Fig. 2 but for HD($v' = 2, j' = 5$) + H reaction product.

possible. One can minimize the sum

$$S = \sum_{i=1}^{i=N} \left(I(\theta_i)^{\text{theory}} - F \cdot I(\theta_i)^{\text{experiment}} \right)^2 \tag{9}$$

with respect to F to obtain the best fit in a least-squares mathematical sense. We have discussed the pitfalls of such a straightforward minimization of the difference of squares in Eq. (9) in Ref. [41]. This is particularly relevant when theory and experiment have pronounced disagreements. The goal of the present study, however, is to compare independently theoretical reactive, inelastic, and reactive + inelastic calculations to experimental measurements and see which one of these three curves best matches the measurement. We therefore stick to a straightforward calculation of an F value for

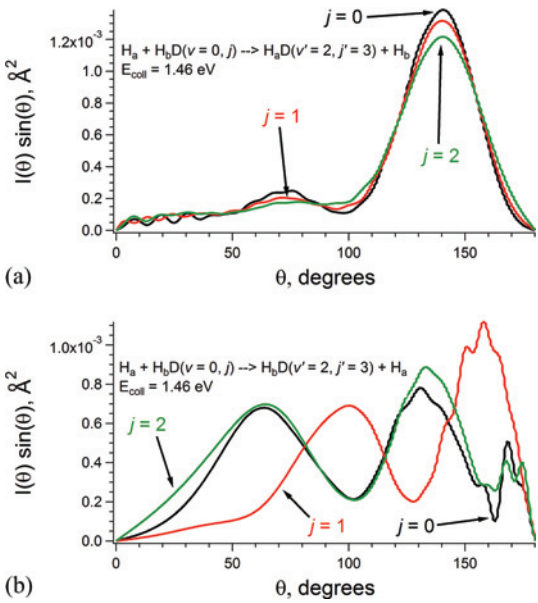

Fig. 7. Calculated DCS for **(a)** reactive and **(b)** inelastic $H + HD(v = 0, j) \rightarrow HD(v' = 2, j' = 3) + H$ scattering. Initial rotational state of HD reactant does not affect the overall shape of a reactive DCS, whereas it has dramatic effects in the case of inelastic scattering.

Table 2. The quality of fits, as described by R^2 values, as well as the uncertainty in the fit parameter F, $\delta F/F$, of $HD(v', j')$ states shown in Figs. 2–6. For all states studied, the $|f_R|^2 + |f_{NR}|^2$ fit is better than either $|f_R|^2$ or $|f_{NR}|^2$, as indicated by how close the R^2 values are to unity.

$HD(v', j')$ state	$\lvert f_R\rvert^2 + \lvert f_{NR}\rvert^2$ R^2	$\lvert f_R\rvert^2 + \lvert f_{NR}\rvert^2$ $\delta F/F$, %	$\lvert f_R\rvert^2$ R^2	$\lvert f_R\rvert^2$ $\delta F/F$, %	$\lvert f_{NR}\rvert^2$ R^2	$\lvert f_{NR}\rvert^2$ $\delta F/F$, %
(1, 8)	0.96	3.6	0.86	7.6	0.81	8.7
(1, 12)	0.89	7.4	0.76	12.0	0.54	18.7
(1, 13)	0.76	10.0	0.43	15.4	0.37	16.2
(2, 3)	0.97	4.1	0.91	7.3	0.88	8.5
(2, 5)	0.97	4.0	0.89	7.5	0.93	6.2

which $\partial S/\partial F = 0$. We quantify the quality of fits by introducing an R^2 value [41]

$$R^2 \equiv 1 - \frac{\sum_{i=1}^{i=N} \left(I(\theta_i)^{\text{theory}} - F_{\text{best}} \cdot I(\theta_i)^{\text{experiment}}\right)^2}{\sum_{i=1}^{i=N} \left(F_{\text{best}} \cdot I(\theta_i)^{\text{experiment}}\right)^2} \tag{10}$$

where F_{best} is the value for which $\partial S/\partial F = 0$. The resultant R^2 values for reactive, inelastic, and reactive + inelastic fits are shown in Table 2. A perfect fit corresponds to $R^2 = 1$.

5. Discussion

Visual examination of Figs. 2–6 makes it quite clear that the experimental signal is indeed a (incoherent) sum of reactive and inelastic channels – the measured data fit the theoretically calculated sum of reactive and inelastic DCS much better than either reactive or inelastic DCS separately. This is further supported by R^2 values tabulated in Table 2. In all cases $R^2(|f_R|^2+|f_{NR}|^2)$ is greater than $R^2(|f_R|^2)$ or $R^2(|f_{NR}|^2)$. In other words, the $|f_R|^2+|f_{NR}|^2$ fit is in all cases mathematically superior to either the $|f_R|^2$ or $|f_{NR}|^2$ fits. We also point out that in all cases $\delta F/F$, the uncertainty in the fit parameter, is smaller for the $|f_R|^2+|f_{NR}|^2$ fit than for either $|f_R|^2$ or $|f_{NR}|^2$ fits. We believe the above arguments to be in a very strong support for the contention that both reactive and inelastic processes are happening and being detected in the $\mathrm{H}+\mathrm{HD}\rightarrow\mathrm{HD}(v',j')+\mathrm{H}$ reaction.

A few words should also be said about the absolute R^2 values in Table 2. For $\mathrm{HD}(v'=1,j'=8)$, $\mathrm{HD}(v'=2,j'=3)$ and $\mathrm{HD}(v'=2,j'=5)$ states the agreement between experiment and $|f_R|^2+|f_{NR}|^2$ theory is excellent – as attested by R^2 values of 0.96, 0.97, and 0.97, respectively. Visual inspection of the DCSs in Fig. 2, 5, and 6 confirms this. Two highly rotationally excited states, namely $\mathrm{HD}(v'=1,j'=12)$ and $\mathrm{HD}(v'=1,j'=13)$, have somewhat lower R^2 values for $|f_R|^2+|f_{NR}|^2$ fits – 0.89 and 0.76, respectively. This becomes more obvious from Figs. 3 and 4. Even so, the $|f_R|^2$ and $|f_{NR}|^2$ fits are even worse, as can be seen from lower R^2 values in Table 2 and fits in Figs. 3 and 4. On the other hand, the fact that DCSs for highly rotationally excited $\mathrm{HD}(v'=1,j'=12)$ and $\mathrm{HD}(v'=1,j'=13)$ product states show a disagreement between the experiment and theory is completely consistent with our most recent findings in a related $\mathrm{H}+\mathrm{D}_2\rightarrow\mathrm{HD}(v',j')+\mathrm{D}$ reaction, wherein $\mathrm{HD}(v'=0,j'=12$–$15)$ and $\mathrm{HD}(v'=1,j'=12)$ product's DCS showed very similar disagreement between theory and experiment [41]. The source of this discrepancy has not yet been established.

As mentioned previously, we have discovered a very intriguing dependence of the inelastically scattered $\mathrm{HD}(v',j')$ product's DCS on the initial rotational state of the $\mathrm{HD}(v,j)$ reactant. The reactant's rotational state seemed to have played a small role in the case of $\mathrm{H}+\mathrm{D}_2(v=0,j=0,1,2)\rightarrow\mathrm{HD}(v',j')+\mathrm{D}$ collisions; see, for example, Fig. 2 of Ref. [8]. Indeed, we find an almost identical behavior in the case of $\mathrm{H_a}+\mathrm{H_b D}(v=0,j=0,1,2)\rightarrow\mathrm{H_a D}(v',j')+\mathrm{H_b}$ reactive scattering (Fig. 7a) – the DCS for $\mathrm{HD}(v'=2,j'=3)$ is only slightly affected by the reactant HD diatomic being in $j=0$, $j=1$ or $j=2$ rotational state. The DCSs for an inelastic channel, Eq. (1b), however, show a tremendous dependence on the initial rotational state of $\mathrm{HD}(v,j)$ reactant (Fig. 7b). It is clear that the shape of the DCS for $\mathrm{H_a}+\mathrm{H_b D}(v=0,j=0$ and $2)\rightarrow\mathrm{H_b D}(v',j')+\mathrm{H_a}$ reactions is rather similar to each other, whereas the $\mathrm{H_a}+\mathrm{H_b D}(v=0,j=1)\rightarrow\mathrm{H_b D}(v',j')+\mathrm{H_a}$ reaction exhibits a very different behavior – the maxima in the DCS of $\mathrm{H_a}+\mathrm{H_b D}(v=0,\text{even } j)\rightarrow\mathrm{H_b D}(v',j')+\mathrm{H_a}$ reactions correspond to minima in the DCS of $\mathrm{H_a}+\mathrm{H_b D}(v=0,\text{odd } j)\rightarrow\mathrm{H_b D}(v',j')+\mathrm{H_a}$ collisions, and *vice versa*. This behavior was a rather puzzling observation at first, particularly because the HD molecule is composed of different nuclei and, unlike H_2 and D_2 isotopes, does not exist in *para* and *ortho* forms that could account for well-known variations in experimental observables as a function of a rotational quantum number j. Instead, such even j/odd j alterations in the DCS can be explained in terms of parity arguments [42–

44]. We intend to discuss the origin of such remarkable out-of-phase oscillations in the DCSs in a future publication. Briefly, in $H + D_2$ and $H + H_2$, all trajectories occur in symmetric pairs with respect to the angles γ and $\pi - \gamma$, where γ is the angle subtended between the internuclear axis and a line connecting the incoming atom to the center of mass of the diatomic target. In a simple picture, the pairs arise from which end of the diatomic molecule the incoming atom interacts with. Hence the two scattering paths leading to the same final state either interfere completely in a constructive manner (j even to j' even and j odd to j' odd) or completely in a destructive manner (j even to j' odd and j odd to j' even). For HD the center of mass about which the molecule rotates is not located at the center of the molecule, causing both in-phase and out-of-phase interference to survive and not to cancel. Consequently, if the in-phase combination gives rise to a peak at a scattering angle θ, then the out-of-phase combination will give a trough.

Finally, we turn our attention to the last member in Eq. (4), *i.e.*, the interference term $f_{NR}^* f_R + f_R^* f_{NR}$. We have knowingly omitted it when plotting theoretical DCSs in Figs. 2–6. The oscillatory structure introduced by the $f_{NR}^* f_R + f_R^* f_{NR}$ term is small and beyond our experimental resolution, at least for the five states studied here. As mentioned in Sect. 3, the sole effect of the GP at the energies considered here is to modify the sign of f_{NR} relative to f_R. Thus, if GP is taken into account, Eq. (4) should be modified to read

$$\frac{d\sigma}{d\Omega}^{\text{NGP}} = |f_R|^2 + |f_{NR}|^2 + \frac{1}{2}\left(f_{NR}^* f_R + f_R^* f_{NR}\right) \tag{11a}$$

$$\frac{d\sigma}{d\Omega}^{\text{GP}} = |f_R|^2 + |f_{NR}|^2 - \frac{1}{2}\left(f_{NR}^* f_R + f_R^* f_{NR}\right) \tag{11b}$$

Figure 8 plots theoretical HD($v' = 2, j' = 3$) and HD($v' = 2, j' = 5$) DCSs computed without and with the GP effect, abbreviated as 'GP', and 'NGP', respectively, along with experimental measurements. Out of the five states studied, the HD($v' = 2, j'$) products exhibit the largest differences between the GP and NGP DCSs. A close examination of Fig. 8 makes it quite clear that current experimental measurements do not permit an unequivocal confirmation of superiority of either GP or NGP fits. Interestingly enough, this is not an entirely experimental-resolution issue, as one might think at first. Two factors are at play. First, the uncertainty in the scattering angle, $\Delta\theta$, as given by Eq. (7), is in fact quite small in the $\sim 50°$–$150°$ region. For the five states studied, $\Delta\theta \sim \pm 3°$. The oscillations in the GP and NGP DCS in the 50°–150° region is about 10° , as can be seen from Fig. 8. Thus, the inherent $\Delta\theta$ arising from electron recoil does not preclude the possibility of resolving these fast oscillations. There is, however, another factor that must be taken into account when constructing experimental DCSs. The number of experimental points in the DCS, or bins, is dictated by the magnitude of the laboratory speed range, *i.e.*, the size of

$$\text{“Speed range”} = (|\mathbf{u}_{\text{COM}}| + |\mathbf{u}_{\text{HD}}|) - (|\mathbf{u}_{\text{COM}}| - |\mathbf{u}_{\text{HD}}|) \tag{12}$$

This quantity, together with the HD recoil speed imparted by the photoelectron, dictates the maximum number of bins that can be used to construct a particular DCS,

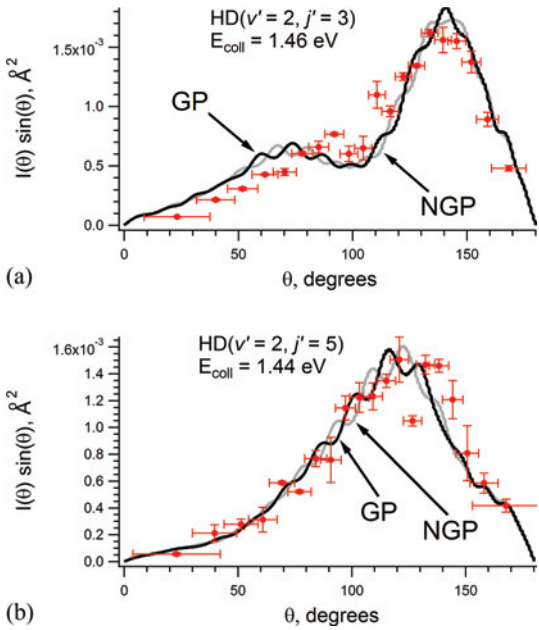

Fig. 8. DCS for (a) HD($\nu' = 2$, $j' = 3$) and (b) HD($\nu' = 2$, $j' = 5$) reactions products. The red dots are an experimental measurement and have the same meaning as in Fig. 2. The two theoretical curves, the GP DCS (black curve), and the NGP DCS (grey), have been computed according to Eqs. (11a) and (11b), respectively. The blurring of theoretical calculations is analogous to that of DCS in Fig. 2.

via

$$\text{“Number of bins”} \leq \frac{\text{“Speed range”}}{\text{HD recoil speed}} \tag{13}$$

For example, in the case of HD($\nu' = 2$, $j' = 3$) and HD($\nu' = 2$, $j' = 5$) states shown in Fig. 8, speed ranges and HD electron recoils are 5824 m/s and 182 m/s and 5238 m/s and 183 m/s, respectively (see Table 1). According to Eq. (13), a maximum of 32 bins can be used for the construction of the HD($\nu' = 2$, $j' = 3$) DCS and 28 for the HD($\nu' = 2$, $j' = 5$) DCS. In such an ideal case, the bins in the backward and sideways direction could be separated by less than 3° in the DCS of HD($\nu' = 2$, $j' = 3$). In case of more internally excited HD($\nu' = 2$, $j' = 5$) reaction products, the spacing in the backward/sideways direction could be around 3.5°. Once again, this is still less than the $\sim 10°$ oscillations in the theoretical GP and NGP DCSs, and, ideally, it should be possible to resolve the two curves in Fig. 8! An obstacle is the fact that a finite number of HD^+ ions are collected. In this case, larger numbers of bins or experimental points lower the number of ions in a particular bin. This leads to larger uncertainties (y-axis error bars). The DCSs presented in Figs. 2–6 and Fig. 8 are therefore a compromise wherein the maximum number of bins were used while keeping the ordinate error bars reasonably small. Even with 20 experimental points in Fig. 8, the spacing between adjacent points in the backward/sideways region of the DCS is about 6° – still less than the

oscillations in theoretical DCS. It should become clear from the above arguments that the experimental resolution cannot be the sole culprit of seemingly identical experimental fits to GP and NGP calculations. Instead, the reason might be very simple indeed: *the precision of experimental measurements is too low* in the present study. Curiously enough, the experimental DCSs for HD($v' = 1, j'$) states seem to have somewhat higher precision, and an even greater number of bins (30, in the case of HD($v' = 1, j' = 8$)); however, the theoretical GP and NGP DCS for these HD($v' = 1, j'$) products are almost indistinguishable.

For the sake of completeness we have carried out the least-squares fitting procedure for both HD states in Fig. 8. In the case of HD($v' = 2, j' = 3$) reaction channel, the R^2 values for GP and NGP fits are $R^2_{\mathrm{GP}} = 0.9683$ and $R^2_{\mathrm{NGP}} = 0.9667$, respectively, where the uncertainties in the R^2 values certainly exceed the difference between them. For the HD($v' = 2, j' = 5$) product state $R^2_{\mathrm{GP}} = 0.9685$ and $R^2_{\mathrm{NGP}} = 0.9657$. In other words, the fit of experimental data to theoretical calculations of GP and NGP DCS are basically identical. Thus, once again nature conspires to hide the geometric phase effect from our preying eyes.

6. Conclusions

We have presented an overwhelming amount of support for the fact that the $\mathrm{H + HD \rightarrow HD}(v', j') + \mathrm{H}$ reaction does indeed proceed *via* two mechanisms – reactive scattering, Eq. (1a), and inelastic scattering, Eq. (1b). This is most easily seen by visually examining the DCS in Figs. 2–6. The fit of experimental data to reactive + inelastic calculations is much better than the fits to either reactive or inelastic calculations, alone. This has been also quantified with least-squares fitting (Table 2). In all cases the R^2value for the reactive + inelastic fit is higher than the R^2 values for either reactive or inelastic fits. It is quite remarkable that the $\mathrm{H + HD \rightarrow HD}(v', j') + \mathrm{H}$ reaction is the first experimental example of its kind, in a way that reactive and inelastic processes have been detected at the same time. This is despite the fact that McCurdy and Miller [42] have derived a general formula for this type of reaction, equations (3) and (4), just over 35 years ago.

We also point out the most curious behavior observed in the DCS of $\mathrm{H_a + H_bD \rightarrow H_bD}(v', j') + \mathrm{H_a}$ inelastic collisions (Fig. 7b). While the reactive $\mathrm{H_a + H_bD \rightarrow H_aD}(v', j') + \mathrm{H_b}$ encounters' DCSs depend weakly on the initial rotational state of HD reactant (Fig. 7a), DCSs of inelastically scattered HD(v', j') products show a very strong dependence on HD reactant's rotational quantum number. We have tentatively attributed this effect to the total parity of the system and whether the change in the rotational angular momentum, $\Delta j = j' - j$, is even or odd.

The GP presence and its manifestation in the $\mathrm{H + H_2}$, $\mathrm{H + D_2}$ and $\mathrm{D + H_2}$ reactions [28,45,46] has been the subject of a considerable controversy among theorists and experimentalists. Calculations by Kuppermann and co-workers in the early 90s predicted significant differences in experimental observables between calculations ignoring and including the GP effect [47,48]. Experimental measurements however were a very good fit to theory that did not take the GP into account [2,7–9,12,49]. Following earlier work by Kendrick [50], Althorpe and co-workers [33,37,38,51,52] succeeded

in proving definitively that the GP has no effect on the ICS and only a minor effect on the DCS at $E_{\mathrm{coll}} < \sim 4$ eV. Instead, noticeable differences in the GP and NGP DCS can be either observed at $E_{\mathrm{coll}} > \sim 4$ eV for any isotopic analogue of the $\mathrm{H} + \mathrm{H}_2$ reaction [37,38] or at any E_{coll} for a reaction like $\mathrm{H} + \mathrm{HD} \rightarrow \mathrm{HD}(\nu', j') + \mathrm{H}$ wherein both reactive and inelastic channels contribute [50,53,54]. In this respect, the current work is the first serious, albeit unsuccessful, attempt to find the geometric phase effect using the indistinguishability of nuclei.

References

1. R. Gotting, H. R. Mayne, and J. P. Toennies, J. Chem. Phys. **80** (1983) 2230.
2. E. Wrede and L. Schnieder, J. Chem. Phys. **107** (1997) 786.
3. L. Schnieder, K. Seekamp-Rahn, E. Wrede, and K. H. Welge, J. Chem. Phys. **107** (1997) 6175.
4. L. Banares, F. J. Aoiz, V. J. Herrero, M. J. D'Mello, B. Niederjohann, K. Seekamp-Rahn, E. Wrede, and L. Schnieder, J. Chem. Phys. **108** (1998) 6160.
5. F. Fernandez-Alonso, B. D. Bean, R. N. Zare, F. J. Aoiz, L. Banares, and J. Castillo, J. Chem. Phys. **115** (2001) 4534.
6. B. D. Bean, J. D. Ayers, F. Fernandez-Alonso, and R. N. Zare, J. Chem. Phys. **116** (2002) 6634.
7. K. Koszinowski, N. T. Goldberg, J. Zhang, R. N. Zare, F. Bouakline, and S. C. Althorpe, J. Chem. Phys. **127** (2007) 124315.
8. N. C.-M. Bartlett, J. Jankunas, T. Goswami, R. N. Zare, F. Bouakline, and S. C. Althorpe, Phys. Chem. Chem. Phys. **13** (2011) 8175.
9. J. Jankunas, R. N. Zare, F. Bouakline, S. C. Althorpe, D. Herraez-Aguilar, and F. J. Aoiz, Science **336** (2012) 1687.
10. J. Aldegunde, D. Herraez-Aguilar, P. G. Jambrina, F. J. Aoiz, J. Jankunas, and R. N. Zare, J. Phys. Chem. Lett. **3** (2012) 2959.
11. H. Xu, N. E. Shafer-Ray, F. Merkt, D. J. Hughes, M. Springer, R. P. Tuckett, and R. N. Zare, J. Chem. Phys. **103** (1995) 5157.
12. E. Wrede, L. Schnieder, K. H. Welge, F. J. Aoiz, L. Banares, J. F. Castillo, B. Martinez-Haya, and V. J. Herrero, J. Chem. Phys. **110** (1999) 9971.
13. S. D. Chao, S. A. Harich, D. X. Dai, C. C. Wang, X. Yang, and R. T. Skodje, J. Chem. Phys. **117** (2002) 8341.
14. S. A. Harich, D. X. Dai, C. C. Wang, X. Yang, S. D. Chao, and R. T. Skodje, Nature **419** (2002) 281.
15. S. C. Althorpe, F. Fernandez-Alonso, B. D. Bean, J. D. Ayers, A. E. Pomerantz, R. N. Zare, and E. Wrede, Nature **416** (2002) 67.
16. J. D. Ayers, A. E. Pomerantz, F. Fernandez-Alonso, F. Ausfelder, B. D. Bean, and R. N. Zare, J. Chem. Phys. **119** (2003) 4662.
17. N. T. Goldberg, J. Zhang, D. J. Miller, and R. N. Zare, J. Phys. Chem. A **112** (2008) 9266.
18. S. J. Greaves, D. Murdock, and E. Wrede, J. Chem. Phys. **128** (2008) 164307.
19. X. Shan and J. N. L. Connor, J. Phys. Chem. A **116** (2012) 11414.
20. D. A. V. Kliner, D. E. Adelman, and R. N. Zare J. Chem. Phys. **94** (1991) 1069.
21. A. E. Pomerantz, F. Ausfelder, R. N. Zare, J. C. Juanes-Marcos, S. C. Althorpe, V. S. Rabanos, F. J. Aoiz, L. Banares, and J. F. Castillo, J. Chem. Phys. **121** (2004) 6587.
22. S. J. Greaves, E. Wrede, N. T. Goldberg, J. Zhang, D. J. Miller, and R. N. Zare, Nature **454** (2008) 88.
23. N. T. Goldberg, J. Zhang, K. Koszinowski, F. Bouakline, S. C. Althorpe, and R. N. Zare, P. Natl. Acad. Sci. USA **105** (2008) 18194.
24. P. G. Jambrina, J. Aldegunde, J. F. Castillo, F. J. Aoiz, and V. S. Rabanos, J. Chem. Phys. **130** (2009) 031102.

25. J. Aldegunde, P. G. Jambrina, V. Saez-Rabanos, M. P. de Miranda, and F. J. Aoiz, Phys. Chem. Chem. Phys. **12** (2010) 13626.
26. L. D. Landau and E. M. Lifshitz, *Quantum Mechanics (Non-relativistic Theory)*, 2nd edn., Pergamon Press Ltd., London-Paris (1963), p. 423.
27. J. D. Doll, T. F. George, and W. H. Miller, J. Chem. Phys. **58** (1973) 1343.
28. C. A. Mead, J. Chem. Phys. **72** (1980) 3839.
29. K. Koszinowski, N. T. Goldberg, A. E. Pomerantz, and R. N. Zare, J. Chem. Phys. **125** (2006) 133503.
30. D. Skouteris, J. F. Castillo, and D. E. Manolopoulos, Comput. Phys. Commun. **133** (2000) 128.
31. A. I. Boothroyd, W. J. Keogh, P. G. Martin, and M. R. Peterson, J. Chem. Phys. **104** (1996) 7139.
32. S. C. Althorpe, J. Chem. Phys. **114** (2001) 1601.
33. J. C. Juanes-Marcos and S. C. Althorpe, Chem. Phys. Lett. **381** (2003) 743.
34. J. C. Juanes-Marcos and S. C. Althorpe, J. Chem. Phys. **122** (2005) 204324.
35. J. C. Juanes-Marcos, S. C. Althorpe, and E. Wrede, Science **309** (2005) 1227.
36. F. Bouakline, S. C. Althorpe, and D. Peláez Ruiz, J. Chem. Phys. **128** (2008) 124322 .
37. S. C. Althorpe, J. C. Juanes-Marcos, and E. Wrede, Adv. Chem. Phys. **138** (2008) 1.
38. F. Bouakline, S. C. Althorpe, P. Larregaray, and L. Bonnet, Mol. Phys. **108** (2010) 969.
39. N. E. Shafer, A. J. Orr-Ewing, W. R. Simpson, H. Xu, and R. N. Zare, Chem. Phys. Lett. **212** (1993) 155.
40. F. Fernandez-Alonso, B. D. Bean, and R. N. Zare, J. Chem. Phys. **111** (1999) 1022.
41. J. Jankunas, M. Sneha, R. N. Zare, F. Bouakline, and S. C. Althorpe, J. Chem. Phys. **138**, 094310 (2013).
42. C. W. McCurdy and W. H. Miller, J. Chem. Phys. **67** (1977) 463.
43. C. J. Eyles, M. Brouard, C.-H. Yang, J. Klos, F. J. Aoiz, A. Gijsbertsen, A. E. Wiskerke, and S. Stolte, Nature Chem. **3** (2011) 597.
44. C. J. Eyles, M. Brouard, H. Chadwick, F. J. Aoiz, J. Klos, A. Gijsbertsen, X. Zhang, and S. Stolte, Phys. Chem. Chem. Phys. **14** (2012) 5420.
45. C. A. Mead and D. G. Truhlar, J. Chem. Phys. **70** (1979) 2284.
46. C. A. Mead, Rev. Mod. Phys. **64** (1992) 51.
47. B. Lepetit and A. Kuppermann, Chem. Phys. Lett. **166** (1990) 581.
48. A. Kuppermann and Y.-S. M. Wu, Chem. Phys. Lett. **241** (1995) 229.
49. F. Ausfelder, A. E. Pomerantz, R. N. Zare, S. C. Althorpe, F. J. Aoiz, L. Banares, and J. F. Castillo, J. Chem. Phys. **120** (2004) 3255.
50. B. K. Kendrick, J. Phys. Chem. A **107** (2003) 6739.
51. J. C. Juanes-Marcos, S. C. Althorpe, and E. Wrede, J. Chem. Phys. **126** (2007) 044317.
52. S. C. Althorpe, T. Stecher, and F. Bouakline, J. Chem. Phys. **129** (2008) 214117.
53. Y.-S. M. Wu, A. Kuppermann, and B. Lepetit, Chem. Phys. Lett. **186** (1991) 319.
54. F. Bouakline, B. Lepetit, S. C. Althorpe, and A. Kuppermann, Influence of the Geometric Phase and Non-Adiabatic Coupling on the Dynamics of the $H + H_2$ Molecular System, in: *Springer Series in Chemical Physics 97*, H. Köppel, D.R. Yarkony, H. Barentzen (Eds.), Springer, New York (2010), 201–237.